Carbon 120 (2017) 374–379

Contents lists available at ScienceDirect

Carbon

journal homepage: www.elsevier.com/locate/carbon

A truncated-cone carbon nanotube cold-cathode electron gun

Xuesong Yuan [a, *, 1], Yu Zhang [b, 1], Matthew T. Cole [c], Yang Yan [a], Xiaoyun Li [a], Richard Parmee [c], Jianqiang Wu [a], Ningsheng Xu [b], William I. Milne [c], Shaozhi Deng [b, **]

[a] School of Physical Electronics, University of Electronic Science and Technology of China, Chengdu, 610054, China
[b] State Key Laboratory Optoelectronic Materials and Technologies, Guangdong Province Key Laboratory of Display Material and Technology, School of Electronics and Information Technology, Sun Yat-sen University, Guangzhou, 510275, China
[c] Department of Engineering, Electrical Engineering Division, University of Cambridge, Cambridge, CB3 0FA, United Kingdom

ARTICLE INFO

Article history:
Received 22 November 2016
Received in revised form
13 March 2017
Accepted 14 March 2017
Available online 16 March 2017

ABSTRACT

A concurrently high beam current and high current density carbon nanotube (CNT) cold cathode electron gun is herein developed. A radial electron source has been realized, formed from CNTs synthesized directly on the side walls of a stainless steel truncated-cone electron gun. Experimental results evidenced a 35 kV/50 mA electron beam can achieve a beam transparency of nearly 100% through the use of double anodes and crossed electric and magnetic fields. A maximum beam current density of 3.5 A/cm^2 was achieved. These results demonstrate the potential impact of coupling novel cold cathode gun architectures and emerging nanomaterials and their collective role in augmenting the performance of incumbent electron gun technologies, alongside allowing for the realization new types of field emission vacuum electron radiation sources.

1. Introduction

Vacuum electron radiation sources (VERS) have been applied widely throughout commerce and industry; from national security and space science, to communications and global navigation. Their many functional advantages over their solid-state counterparts, include, in particular, high output power (>1 GW) and high operation frequency (>1 THz) [1,2]. The electron gun is the central component of every VERS device, with most commercially available modern electron guns employing thermionic cathodes. Their high emission current density and stable performance make for robust electrons sources, however; thermionic cathodes suffer from the need for high temperature operation and a have therein a slow temporal response. On the contrary, field emission cold cathodes can be operated at room-temperature, and respond almost instantaneously to local fields, allowing for facile and inexpensive integration alongside aggressive miniaturization.

Carbon nanotubes have proven potential as high performance field emitters in many varied laboratory scale devices [3–5]. The continued maturity of the technology necessitates the proof of principle demonstration of higher technology readiness level devices via systems level design. CNT-based electron sources have been used in flat displays [6,7], X-ray sources [8,9], and travelling wave tubes [10,11]. Compared with Spindt-type field emitter arrays, recent advancements in nanofabrication have allowed for significant cost reductions, coupled to rapid large area manufacturing via advanced chemical vapour deposition (CVD) processes [12,13]. In the present gun the CNTs are grown directly onto the emitter without the need for any functionally deleterious, post-growth wet-chemistry processing. Careful engineering of the growth protocol has allowed us to maximize the degree of adhesion between the CNT and the SS304 substrate, thereby minimizing the degree of CNT removal during operation; an on-going challenge facing nano CVD-based VERS systems.

Nevertheless, various challenges continue to plague CNT-based cold cathode VERS. Central to this is the lack of suitable gun-level architectures that are capable of simultaneously producing high beam currents and high current densities. To date, planar CNT cold cathodes have struggled to obtain beam currents of tens of *mA*, principally due to edge effects, gate losses, emitter degradation and temporal attrition of the emitter [14–17]. In order to obtain large beam currents one viable and common approach is too increase the cathode emission area. Unfortunately increasing the emission area alone often reduces the current density. Indeed, in most cases the

* Corresponding author.
** Corresponding author.
E-mail addresses: yuanxs@uestc.edu.cn (X. Yuan), stsdsz@mail.sysu.edu.cn (S. Deng).
[1] Authors contributed equally to this work.

http://dx.doi.org/10.1016/j.carbon.2017.03.046
0008-6223/

emission current density for larges area devices is often tens to hundreds of mA/cm^2. Although the emission current density of a single carbon nanotube has been shown to be >10^{10} A/m^2 [18], this is largely a product of the very low emission area rather than a concurrently high emission current and high emission area [19–24]. Thus, a second common challenge lies in beam focusing as a means to further increase the emission current density. Such beam compression will also improve the cross-sectional spatial uniformity of the electron beam, though such strategies are often computationally demanding to engineer and challenging to fabricate.

In this paper, a simultaneously high beam current and high current density truncated-cone CNT cold cathode electron gun is demonstrated. Here the CNT electron source is grown directly onto the side walls of a stainless steel truncated-cone, towards realizing a new generation of VERS. Double anodes and crossed electric and magnetic fields are used to obviate edge effects and gate losses resulting in the formation of a radially homogenous annular electron beam whilst also demonstrating the present architectures ability to provide high-compression ratios of more than two orders of magnitude.

2. Results

2.1. Truncated-cone CNT cold cathode diode experiment

In the truncated-cone CNT cold cathode diode experiment, as depicted in Fig. 1A, the anode and cathode were separated by a ceramic spacer some 1 mm thick (Fig. 1B). The right-hand side port is that through which the primary electron beam is emitted. Measurements were performed using pulsed mode operation with a typical pulse duration of 10 ms. The maximum negative output voltage was set to −15 kV, which was connected to earth through resistors R_1 (4 kΩ) and R_2 (36 kΩ), where R_1 is a protection resistor and R_2 is a high-voltage divider resistor. The cathode is connected to the negative high voltage and the anode is connected to the earth through the protection resistor R_p and a test resistor R_{test} (106 Ω). Through probing the voltage across R_{test} using an oscilloscope (HP infinium) we calculate the beam current. The truncated-cone CNT diode source in mounted in a vacuum chamber at 9 × 10^{-5} Pa. U_a is the actual voltage applied on CNT cold cathode, which can be calculated by:

$$U_a = U_0\frac{R2}{R1+R2} - I(R_p + R_{test}) \quad (1)$$

where U_0 is the power supply output voltage, and I is the field emission current given by U_{test}/R_{test}, where U_{test} is the oscilloscopes second channel monitor. Using this method we observe clear emission stabilization characteristics in single high voltage pulse process. Fig. 1C shows the experimental setup. The cathode height was 9.8 mm, with a top and bottom radii of 8.0 mm and 8.5 mm, respectively. The total area of the CNT cold cathode was 5.08 cm^2. The inner wall of the anode lies parallel to the outer wall of the cathode, with the cathode lying coaxial within the anode. The distance between anode and cathode was 1 mm. By changing the cathode position along the axis, the inter-electrode separation can be accurately adjusted with a resolution of 50 μm per mm of lateral travel. Fig. 1D shows typical emission currents as a function of the applied voltage. The three typical test profiles correspond to; before the forming processing (square), after the forming processing (circle), and after 2 h continuous operation (triangle). The low initial field emission performance is a result of but a few carbon nanotubes (approx. 10% of the population) emitting. The subsequent forming processing profile is associated with the CNT cathode that has been processed with short high voltage pulses (7.5 kV/100 μs). The maximum emission current achieved was 103 mA for the treated samples, where this treatment effectively activated a greater proportion of the CNT population. The continuous operation profile shows the emission performance after 2 h pulsed operation. Here, the operation current was about 70 mA at 1 Hz. To investigate the robustness of the present sources, we increased, significantly, the operation voltage of the continuous samples following the 2 h experiment. Notable high voltage arcing occurred for fields in excess of 8.3 V/μm, with post-SEM analysis showing serious degradation of the CNT.

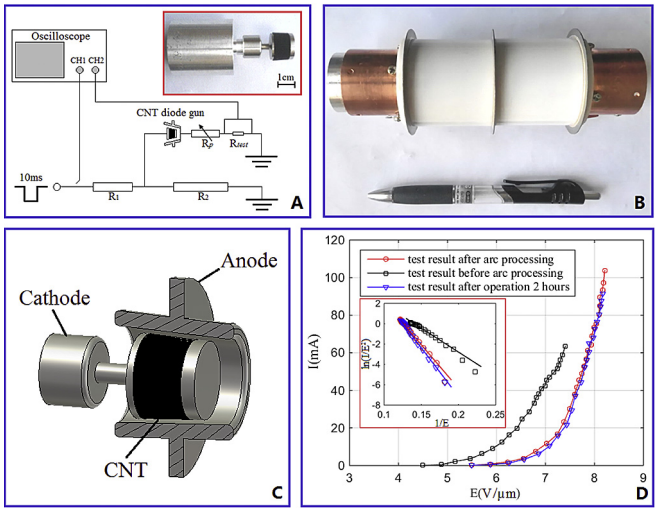

Fig. 1. Truncated-cone CNT cold cathode diode experiment. (A) Experimental schematic, inset: photo of a typical fabricated truncated-cone CNT cold cathode. (B) Photo of the complete truncated-cone CNT cold cathode diode gun. (C) Scheme of the truncated-cone CNT cold cathode coaxial diode. (D) Experimental field emission current as a function of anode voltage, inset: Fowler-Nordheim plots. (A colour version of this figure can be viewed online.)

2.2. Truncated-cone CNT cold cathode electron gun experiment

The CNT truncated-cone gun was mounted in a ceramic (99% Al_2O_3), fully-sealed vessel evacuated to a base pressure of <10e^{-7} *Pa* prior to sealing in a double-vacuum baked device. The distance between the cathode and control anode is 1.3 mm. The length of the anode is 245 mm. At the gun output port a sapphire (Al_2O_3) window was used to seal the unit. To observe the electron beam spot dimensions, an ITO-coated glass electrode was fixed in the front of the output window with a single lens reflex camera mounted some 5 mm distant. Fig. 2A shows the electron gun scheme. The CNT-coated truncated-cone was produced by directly synthesising the CNT by thermal chemical vapour deposition on the catalytically active stainless steel (SS304) substrate. Type SS304 was selected over other steel types given its low cost and its high proportion of CNT suitable catalytically active species; chiefly, iron (60%), and nickel (8%). Fig. 2C shows a photograph of the sealed CNT cold cathode. In order to decrease edge effects along the tubes long axis, the CNT cold cathode is sandwiched between two stainless steel truncated-cones. To avoid contamination, the CNT was grown on the central section independently, which was latterly installed in the tube. Fig. 2D shows a typical SEM micrograph of the as-grown CNT. The CNT had a uniform areal coverage and had a typical diameter between 20 and 50 nm.

Experiments were performed using high voltage pulses some 100 μs in duration, operated at a pulse frequency of 1 Hz. The electron gun was installed in a custom-built 9.2 T superconducting

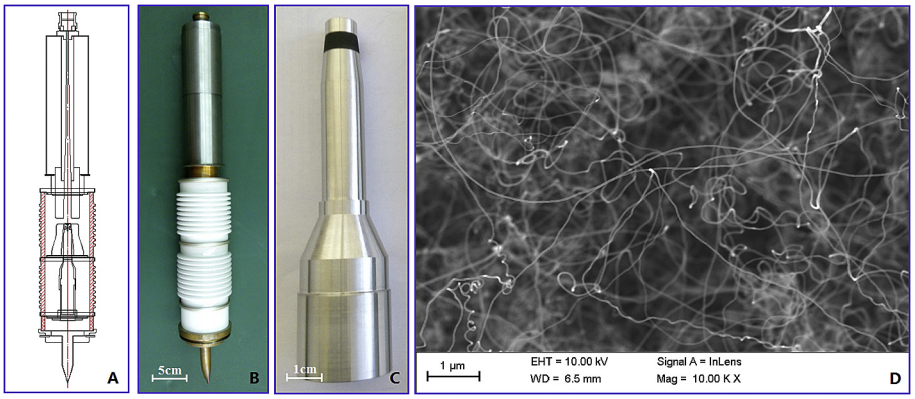

Fig. 2. Truncated-cone CNT cold cathode electron gun. (A) Scheme of truncated-cone CNT cold cathode electron gun. (B) Photograph of truncated-cone CNT cold cathode electron gun. (C) Photograph of CNT cold cathode. (D) SEM micrograph of the typical as-grown CNT. (A colour version of this figure can be viewed online.)

magnetic system. The profile of the magnetic field intensity along the tube central axis is shown in Fig. 4B. −35 kV was divided to provide the negative high voltage for the cathode and control anode. The anode was connected to earth through a test resistance, R_{test} (475 Ω). The bias on R_{test} was recorded with a dual channel oscilloscope (HP infinium) and the beam current therein extracted. We observe clear emission stabilization within a single high voltage pulse. A typical emission current profile is shown in Fig. 3A. An example image of the electron beam spot is shown in the insert of Fig. 3A. The average radius of the beam was about 1.1 mm, giving an experimental compression ratio of approximately 100. The typical beam current, as a function of the voltage difference between cathode and control anode, is shown in Fig. 3B. The maximum beam current was around 50 mA. Fig. 3C shows the pulsed emission stability under varied operation frequencies. Here, the electric field was 7.5 V/μm and the pulse duration was 100 μs. The initialization emission current was about 25 mA. Between 0 and 6 h the operation frequency was 1 Hz and the emission current remained unchanged. Then, the emission current decreased by 4% after 6 h operating at a pulse frequency of 10 Hz. When the operation frequency was further increased to 100 Hz, the emission current decreased by a further 35% over the subsequent 6 h. Experimental results of pulsed emission stability show a low robustness operating at a pulse frequency of 100 Hz. However, the lower the operation frequency is, the longer its life-time will be with the same operating voltage. Thus, when the CNT cold cathode operates at a pulse frequency of 1 Hz and the mission current decreases by 8%, the life-time will be more than 120 h.

2.3. Simulation results

A major advantage of the proposed truncated-cone architecture is the high compression ratio. Here we investigated this functional feature as a means to realize a 220 GHz gyrotron radiation source [25]. The high compression truncated-cone gun is designed using commercially available 3D simulation software (CST). Given the semi-metallic nature of the misaligned CNT, the basic field emission process is suitably well described by a generalised Fowler-Nordheim equation, of the form: $J = AE^2 \exp(-B/E)$. Here A and B are the approximate Fowler-Nordheim constants, which are estimated according to our previous experimental results [26,27]. In order to obtain a high compression ratio, a strong axial magnetic field is required. Fig. 4A shows the simulated beam trajectories under a field of 8.4 T operating at 35 kV/50 mA. The coaxial cathode and control anode are depicted in inset (2). Here we increased the top and bottom radii of the truncated-cone which we set as 4.2 mm and 4.7 mm, respectively. The height of cathode was 5 mm. The distance between the cathode and control anode was 1.3 mm. An inter-electrode gap, $d_g = 0.8$ mm was used to allow the electron beam to pass through the cavity efficiently. The total gun length was 260 mm. The left end axial position is defined as z = 0 mm. Fig. 4B shows the profile of the magnetic field intensity along the central axis, which was obtained based on the experimental magnetic field system. In the cathode region the magnetic field B_c is approximately 0.5 T. At the beam output port, the magnetic field B_0 is 8.4 T.

The primary emission area was 44.7π mm^2. Changing this area (side wall of the truncated-cone) into a plane ring gives an inner radius of 4.2 mm. The outer radius reaches 7.9 mm, as illustrated in Fig. 5A. Fig. 5B shows the beam spot cross-section at z = 26 mm (anode input port). The inner and outer radii of the beam spot are 4.2 mm and 4.7 mm, respectively. Fig. 5C shows the beam cross-section at z = 260 mm (gun output port). The system is designed to mediate two-stage compression. Firstly, the emitted electrons move towards the control anode, here beam gyration/helical motion occur along the magnetic field line. The first-stage

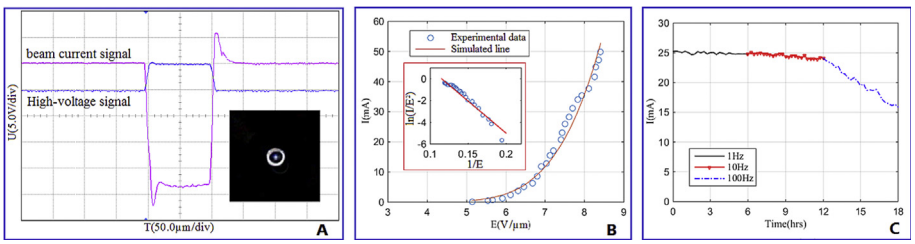

Fig. 3. Experimental results of truncated-cone CNT cold cathode electron gun. (A) A typical test curve of beam current signal and high-voltage on oscilloscope, inset: beam spot on ITO-coated glass. (B) Experimental results of electron beam current as a function of electric field, inset: Fowler-Nordheim plot. (C) Pulsed emission stability of CNT cold cathode with different operation frequencies (1 Hz, 10 Hz and 100 Hz). (A colour version of this figure can be viewed online.)

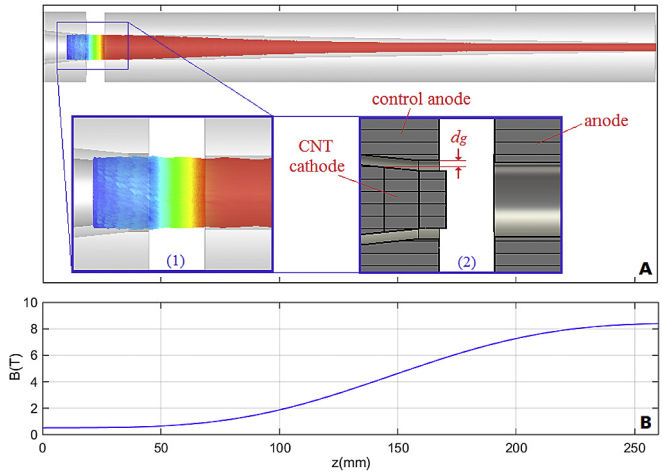

Fig. 4. Beam trajectories within the CNT truncated-cone electron gun. (A) Simulated beam trajectories, inset (1): expanded view of the primary emission zone, inset (2): cross-sectional view of the structure. (B) Magnetic field intensity profile along the tube central axis. (A colour version of this figure can be viewed online.)

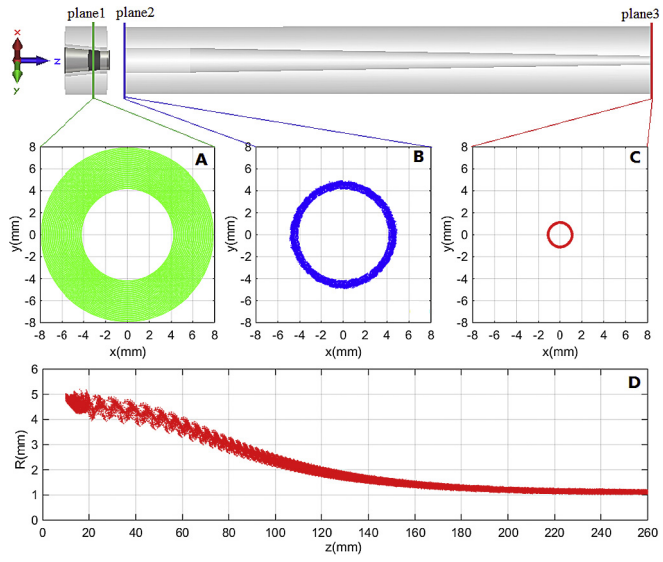

Fig. 5. Electron phase space. (A) CNT cold cathode emission area in plane 1, (B) in plane 2 (z = 26 mm), (C) in plane 3 (z = 260 mm). (D) Beam inner and outer radii as a function of axis. (A colour version of this figure can be viewed online.)

compression is completed at the anode input port. The electron beam cross-section is compressed from the cold cathode emission area (44.7π mm^2) into a beam spot approximately 4.45π mm^2, (Fig. 5B). In this first compression process, the magnitude of the magnetic field is almost unchanged and the electron beam current density is increased tenfold. In the second compression stage, the electron beam transits past the anode. The electric field here is largely unchanged whilst the magnetic field is increased. The beam is adiabatically compressed by the magnetic field. The radius of the electron beam starts to decrease, at an increasing rate, as a function of axial length. At the gun output port the inner and outer radii of electron beam are 1.0 mm and 1.2 mm, respectively. The electron beam cross-sectional area reduces from 4.45π mm^2 to 0.44π mm^2 (Fig. 5C). At the gun exit port the electron beam cross-sectional area is compressed by approximately 100 times, with the beam current density correspondingly enhanced by a comparable amount. Fig. 5D shows the beam inner and outer radii as a function of axis position. As illustrated in Fig. 4B, we can find the beam centre radius is about 1.5 mm at z = 150 mm and the magnetic field at this position is only 4.8 T.

3. Materials and methods

Obtaining high emission currents is an evident prerequisite to realize an emerging class of advanced vacuum electron radiation sources. Here we achieve an increased beam current by increasing the effective emission area through the use of a truncated-cone cathode architecture. In the present system the CNTs are grown on the side walls of a SS304 truncated-cone through the use of thermal chemical vapour deposition, as reported in detail elsewhere [28]. The CNT growth was conducted for 10 min in a high temperature furnace operated at 750 °C (35 °C/min) under an atmosphere of ethylene (20 sccm, purity 99.9%), hydrogen (200 sccm, purity 99.9%), and argon (200 sccm, purity 99.9%) at near atmospheric pressure.

The cathode (inner conductor) and anode (outer conductor) are coaxial and the side wall of the cathode is parallel to the inner side wall of anode in the truncated-cone model, shown in Fig. 6A. When a high electric potential is set on the anode, the electrons emit from the CNT via cold cathode emission. The electrons principally emit perpendicular to the cathode surface. For a given cone-angle θ, the electron velocity consists of an axial and vertical component. Emitted electrons tend to gyrate along the magnetic flux line whilst propagating in the axial direction. For a larger cone-angle the vertical velocity decreases and the radius of gyration of the electrons (the beam undulation) will decrease with the same operation magnetic field amplitude. Thus, the operation magnetic field amplitude can be lowered. When θ tends towards 90°, the truncated-cone model approaches a more conventional parallel plate system. Under such circumstances, magnetic fields are no longer necessary, but significant apertures must be opened within the anode to facilitate beam propagation. This model encompasses conventional Spindt-type systems. In such systems the uniformity and strength of the electric field at the cold cathode surface is severely inhibited, with significant deleterious beam bombarding effects occurring at the anode. On the contrary, there is no requirement for apertures in the anode in the present truncated-cone architecture, reducing the need for costly, high precision laser or water-jet cutting. The electric field on the cold cathode surface is comparatively more uniform and the strength of the electric field on the cathode surface is thereby enhanced. In an infinite parallel plate model, the electric field uniform distribution between two plates and the electrostatic field is obtained from $E = U/d$. Here U is the electric potential difference between two plates, and d is the distance between the plates. In an infinite length coaxial model, the electric field is compressed on the surface of the inner conductor (cathode), giving $E = U/(R^*\ln(R_a/R_c))$. Here R is the radial position, and R_c and R_a are the cathode and anode radii, respectively. When $R = R_c$ and $d = (R_a\text{-}R_c)$, the potential difference in the two cases are equivalent. The field enhancement factor β of the infinite length coaxial model, as compared to the infinite plate model, is $\beta = (R_a\text{-}R_c)/(R_c\ln(R_a/R_c))$. Fig. 6B shows electrostatic field simulations of the truncated-cone operated in diode mode. In order to decrease edge effects along the axis, the CNT cold cathode is sandwiched by two radially nested, and axially separated truncated-cones. The CNT cathode is located at the midpoint. The total height of three sections is 10 mm. The height of the CNT cathode is 6 mm. θ of three truncated-cones is equivalent. The top and bottom radii of the truncated-cones are 1.0 mm and 1.5 mm, respectively. The top and bottom radii of inner wall of anode are 11.0 mm and 11.5 mm, respectively. The height of the anode is 10.0 mm. The distance between cathode and anode is 10.0 mm. The

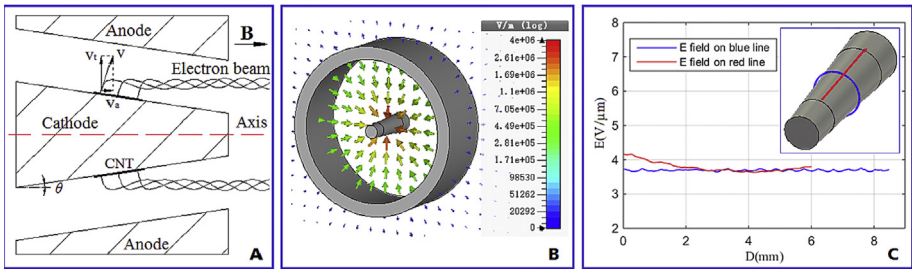

Fig. 6. Truncated-cone CNT cold cathode model. (A) Truncated-cone cold cathode electron gun model. (B) Simulation results of electrostatic field on cross-section, (C) electrostatic field amplitude on two blue lines on cathode surface. (A colour version of this figure can be viewed online.)

potential difference between the cathode and anode is 10 kV. The anode is grounded. Based on this potential difference, an electric field of 1.0 kV/mm is anticipated in the two plate diode model. However, an electric field of about 3.6 kV/mm is anticipated in the truncated-cone model. Our finite element modelling suggests electric fields on the cathode and anode surfaces of 3.68 kV/mm and 0.43 kV/mm, respectively (Fig. 6B). Fig. 6C shows the electric field at two inspection points on the surface of the cathode (whose positions are depicted in the inset). The electric fields are very notably uniform (blue line, 3.70–3.75 V/μm). The change in the electric field along the longitudinal direction line is also rather small (red line, 3.70–4.10 V/μm), since the radius of the truncated-cone is reduced and the enhancement factor increases.

4. Discussion

Carbon nanotubes can be grown conformally on flat, curved and highly perturbed surfaces [28–30]. It is the former of these, coating of CNT onto planar surfaces, which pose many difficulties and insurmountable processing challenges if Spindt-type CNT field emission cathodes were to be used. In order to increase the intensity of the electric field at the cathode surface, the size of the grid aperture should be minimised. Unfortunately, however, this will likely stimulate a short circuit between the cathode and grid, alongside high grid losses, as well as loss of emission uniformity, all of which are especially difficult to overcome simultaneously. By exploiting emerging CNT growth techniques on curved and coaxial structures, many of these problems are solved immediately. Such design methodologies allow the distance between the cathode and grid (outer conductor) to be as large as necessary whilst also allowing for the electric field on cathode surface to be enhanced. Grid interception and losses therein, are also dramatically reduced since an axial magnetic field and large cathode-grid gap are set. By extending the emission sit area along the axial direction, the effective emission area per unit planar area is much more than that attainable with conventional Spindt-type cold cathodes.

To satisfy the 220 GHz gyrotron operational parameters, we select a magnetic field of 8.4 T. As a result, the present gun design is particularly long relative to a more optimal design and in comparison to other systems. To mediate further axial miniaturization, it is necessary for the magnetic field, as a function of tube length, to increase at a greater rate, though our simulations suggest under such field conditions significant electron back bombardment may occur due to magnetic mirroring effects. The length of electron gun can be shortened if we lower the gyrotron frequency or develop other VERS architectures. In the present gun architecture, only 15 mm separates the input port at the anode tunnel, though a tenfold compression ratio is still achievable. If the current density requirements of any given application can be satisfied at lower compressions, then the length of electron gun can be reduced to around 20 mm. Furthermore, the operation magnetic field is only 0.5 T, which too can be reduced if we increase the distance between cathode and anode.

The truncated-cone CNT cold cathode, as a new architecture towards new VERS paradigms, has merit in application not only in traditional devices but also in new vacuum microelectronic devices. The radii of the truncated-cone CNT cold cathode and control anode are set at 5 μm and 50 μm in a vacuum microelectronic device, respectively. Compared with the parallel plate diode system the electric field on the cathode surface will increase by approximately a factor of four. Compared with comparable grid systems, this is a substantial increase and the electric field on cathode surface is manifestly more uniform. Simultaneously, by increasing the height of the truncated-cone, the emission area will be effectively enlarged. Should only the first-stage compression be necessary, the required magnetic field will be particularly small and easy to realize making it widely appealing to a variety of small-scale vacuum microelectronic devices.

Our studies also suggest that the size of the emission unit can be changed from the μm to the mm scale. Collectively there are manifold functional advantages to the present truncated-cone architecture, including an increased cathode-grid gap, enhanced local electric field decreased requirements on magnetic fields, and reduced grid losses, all of which may assist in the realization of the next generation of nanomaterial-based functionally advanced VERS.

5. Conclusion

A maximum beam peak power of 1.75 kW was measured offering one solution to the on-going issue of low beam power from CNT-based vacuum power electronic devices, whilst simultaneously increasing the beam current density by two orders of magnitude via axial magnetic compression. A fully-sealed electron gun, demonstrated in a 220 GHz gyrotron radiation source, has been developed and through further materials optimization and macro-scale architecture improvements, we believe the present study provides a positive outlook towards realizing CNT-based cold cathode millimetre-wave and terahertz VERS devices, including gyrotrons, travelling wave tubes, and backward wave oscillators.

Acknowledgments

This work was supported by the National Basic Research Program of China (No.2013CB933600), National Natural Science Foundation of China (No.61101041) and Fundamental Research Funds for the Central Universities (Grant No. ZYGX2016J059).

References

[1] Robert J. Barker, Edl Schamiloglu, High-power Mircowave Sources and Technologies, Wiley-IEEE Press, 2001.

[2] V.L. Bratman, Yu. K. Kalynov, V.N. Manuilov, Large-orbit gyrotron operation in the terahertz frequency range, Phys. Rev. Lett. 102 (2009) 245101.
[3] R.H. Baughman, A.A. Zakhidov, W.A. De Heer, Carbon nanotubes—the route toward applications, Science 297 (5582) (2002) 787–792.
[4] Clare M. Collins, Richard J. Parmee, William I. Milne, Matthew T. Cole, High performance field emitters, Adv. Sci. (2016) 1500318.
[5] Grigory S. Bocharov, Alexander V. Eletskii, Theory of carbon nanotube (CNT)-Based electron field emitters, Nanomaterials 3 (2013) 393–442.
[6] Yahachi Saitoa, Sashiro Uemurab, Field emission from carbon nanotubes and its application to electron sources, Carbon 38 (2000) 169–182.
[7] Peng Liu, Yang Wei, Kai Liu, Liang Liu, Kaili Jiang, Shoushan Fan, New-type planar field emission display with super aligned carbon nanotube yarn emitter, Nano Lett. 12 (2012) 2391–2396.
[8] Jin-Woo Jeong, Jae-Woo Kim, Jun-Tae Kang, Sungyoul Choi, Seungjoon Ahn, Yoon-Ho Song, A vacuum-sealed compact x-ray tube based on focused carbon nanotube field-emission electrons, Nanotechnology 24 (2013) 085201.
[9] W. Sugimoto, S. Sugita, Y. Sakai, H. Goto, Y. Watanabe, Y. Ohga, S. Kita, T. Ohara, A fine-focusing x-ray source using carbon-nanofiber field emitter, J. Appl. Phys. 108 (2010) 044507.
[10] H.J. Kim, J.J. Choi, J.H. Han, J.H. Park, J.B. Yoo, Design and field emission test of carbon nanotube pasted cathodes for traveling wave tube applications, IEEE Trans. Electron Dev. 53 (11) (2006) 2674–2680.
[11] Xuesong Yuan, Yu Zhang, Huan Yang, Xiaoyun Li, Ningsheng Xu, Shaozhi Deng, Yang Yan, A gridded high-compression-ratio CarbonNanotube cold cathode electron gun, IEEE Electron Device Lett. 36 (4) (2015) 399–401.
[12] M.T. Cole, W.I. Milne, Plasma enhanced chemical vapour deposition of horizontally aligned carbon nanotubes, Materials 6 (2013) 2262–2273.
[13] N. S. Xu, Jun Chen, S. Z. Deng, J. C. She. The preparation method of carbon nanotubes film on stainless steel substrate, China Patent, ZL02115095.8, 2004.
[14] V. Chouhan, T. Noguchi, S. Kato, Field emission from optimized structure of carbon nanotube field emitter array, J. Appl. Phys. 119 (13) (2016) 134303.
[15] Di Yunsong, Wang Qilong, Zhang Xiaobing, Lei Wei, Du Xiaofei, Yu Cairu, A vacuum sealed high emission current and transmission efficiency carbon nanotube triode, AIP Adv. 6 (4) (2016) 045114.
[16] Ha Rim Lee, Soo Wong Lee, Callixte Shikili, Jung Su Kang, Jong Lee, Kyu Chang Park, Enhanced electron emission of paste CNT emitters with nickel buffer layer and its X-ray application, J. Nanosci. Nanotechnol. 16 (11) (2016) 12053–12058.
[17] Giacomo Ulisse, Claudio Ciceroni, Francesca Brunetti, Aldo Di Carlo, Electrostatic beam focusing of carbon nanotubes electron source, IEEE Trans. Electron Devices 61 (7) (2014) 2558–2563.
[18] J.C. She, N.S. Xu, S.Z. Deng, J. Chen, H. Bishop, S.E. Huq, L. Wang, D.Y. Zhong, E.G. Wang, Vacuum breakdown of carbon-nanotube field emitters on a silicon tip, Appl. Phys. Lett. 83 (13) (2003) 2671–2673.
[19] Valerie J. Scott, Harish Manohara, Risaku Toda, Linda Del Castillo, Rakesh Murthy, Jerry Mulder, Eshwari Murty, M. Clark Thompson, Robust CNT field emitters: patterning, growth, transfer, and in situ anchoring, Nanotechnology 27 (49) (2016) 494002.
[20] Lei Wei, Zhu Zhuoya, Liu Chunyi, Zhang Xiaobing, Wang Baoping, Nathan Arokia, High-current field-emission of carbon nanotubes and its application as a fast-imaging X-ray source, Carbon 94 (2015) 687–693.
[21] Yuning Sun, Yenan Song, Dong Hoon Shin, Ki Nam Yun, Seok-Gy Jeon, Jung-Il Kim, Yahachi Saito, Cheol Jin Lee, Fabrication of carbon nanotube emitters on the graphite rod and their high field emission performance, Appl. Phys. Lett. 104(4) (2014) 043104.
[22] V. Guglielmotti, E. Tamburri, S. Orlanducci, M.L. Terranova, M. Rossi, M. Notarianni, S.B. Fairchild, B. Maruyama, N. Behabtu, C.C. Young, M. Pasquali, Macroscopic self-standing SWCNT fibres as efficient electron emitters with very high emission current for robust cold cathodes, Carbon 52 (2013) 356–362.
[23] Guohai Chen, Suman Neupane, Wenzhi Li, Lina Chen, Jiandi Zhang, An increase in the field emission from vertically aligned multiwalled carbon nanotubes caused by NH3 plasma treatment, Carbon 52 (2013) 468–475.
[24] Sung Mi Jung, Hyun Young Jung, Jung Sang Suh, Horizontally aligned carbon nanotube field emitters having a long term stability, Carbon 45 (2007) 2917–2921.
[25] Xuesong Yuan, Weiwei Zhu, Yu Zhang, Ningsheng Xu, Yang Yan, Jianqiang Wu, Yan Shen, Jun Chen, Juncong She, Shaozhi Deng, A fully-sealed carbon-nanotube cold-cathode terahertz gyrotron, Sci. Rep. 6 (2016) 32936.
[26] Xuesong Yuan, Matthew T. Cole, Yu Zhang, Jianqiang Wu, William I. Milne, Yang Yan, Parametrically optimized carbon nanotube-coated cold cathode Spindt arrays, Nanomaterials 7 (13) (2017) 7010013.
[27] Yuan Xue-Song, Zhang Yu, Sun Li-Min, Li Xiao-Yun, Deng Shao-Zhi, Xu Ning-Sheng, Yan Yang, Study of pulsed field emission characteristics and simulation models of carbon nanotube cold cathodes, Acta Phys. Sin. 61 (21) (2012) 216101.
[28] M.T. Cole, K. Hou, J.H. Warner, J.S. Barnard, K. Ying, Y. Zhang, C. Li, K.B.K. Teo, W.I. Milne, In-Situ deposition of sparse vertically aligned carbon nanofibres on catalytically activated stainless steel mesh for field emission applications, Dia. Rel. Mater. 23 (2012) 66–71.
[29] Wenjing Xu, Shiting Wu, Xinming Li, Mingchu Zou, Liusi Yang, Zelin Zhang, Jinquan Wei, Song Hu, Yanhui Li, Anyuan Cao, High-Efficiency large-area carbon nanotube-silicon solar cells, Adv. Energy Mater. 6 (2016) 1600095.
[30] Haitao Wang, Chongzheng Na, Chemical bath deposition of aluminum oxide buffer on curved surfaces for growing aligned carbon nanotube arrays, Langmuir 31 (2015) 7401–7409.